Post-liquefaction reconsolidation of sand

O. Adamidis[1] and G.S.P. Madabhushi

[1]oa245@cam.ac.uk

Abstract

Loosely packed sand that is saturated with water can liquefy during an earthquake, potentially causing significant damage. Once the shaking is over, the excess pore water pressures that developed during the earthquake gradually dissipate, while the surface of the soil settles, in a process called post-liquefaction reconsolidation. When examining reconsolidation, the soil is typically divided in liquefied and solidified parts, which are modelled separately. The aim of this paper is to show that this fragmentation is not necessary. By assuming that the hydraulic conductivity and the one-dimensional stiffness of liquefied sand have real, positive values, the equation of consolidation can be numerically solved throughout a reconsolidating layer. Predictions made in this manner show good agreement with geotechnical centrifuge experiments. It is shown that the variation of one-dimensional stiffness with effective stress and void ratio is the most crucial parameter in accurately capturing reconsolidation.

1. Introduction

Water saturated deposits of loose sand can liquefy during earthquakes. An intuitive explanation of liquefaction has long been available, suggesting the tendency of loose sands to contract when agitated as the cause (3). During shaking, the water that fills the pores between sand grains must move for contraction to occur. If drainage cannot happen fast enough, excess pore water pressure is produced. The normal forces between grains, and consequently the soil's shear strength, diminish as pore pressure builds up. After the end of the earthquake, excess pore pressure dissipates and water flows upwards, prolonging the time during which the soil at the surface of the layer remains liquefied and structures are at risk. Damage can occur or continue after the end of shaking (9).

The process during which the excess pore water pressure of a liquefied layer gradually dissipates after the end of an earthquake is called reconsolidation. During reconsolidation, the contact forces between sand grains are re-established. The study of reconsolidation is pursued primarily due to the related damage to the built environment. Consequently, the main goal of a reconsolidation analysis is to predict the settlement of the soil surface, which is crucial in assessing the response of structures.

Studying reconsolidation can also further our understanding of liquefied soil. There are important gaps in our understanding of liquefaction, such as the increased settlement rate of liquefied soil during the earthquake, compared to that during reconsolidation (18). Determining the deformation of the soil matrix and its coupling with pore pressures also remains a major issue ((5), (15), (26)). Reconsolidation offers the opportunity to study liquefied soil without the added complexity of dynamic loading. However, much uncertainty remains, even regarding the fundamental mechanism (13). After an exhaustive review of efforts to model liquefaction, it was concluded in (24) that 'little is known about the behavior of liquefied sand, as well as about postliquefaction deformations of saturated sand'. A reconsolidation analysis that manages to

accurately predict the dissipation of pore water pressure can offer valuable insight regarding soil behaviour.

Certain terms of soil mechanics are of use. The total vertical stress at a certain depth is calculated by multiplying the said depth with the unit weight of the soil, including both water and soil grains. The effective stress principle mandates that by subtracting water pressure from total vertical stress, the effective vertical stress can be calculated. Effective stress is a measure of the contact forces between grains. The subtraction of hydrostatic pressure from the current value of pore water pressure gives the excess pore pressure. During reconsolidation, total vertical stresses remain constant and excess pore pressures dissipate. Reconsolidation of homogeneous layers is a one-dimensional phenomenon, for which only vertical stresses are of interest. The term 'vertical' will not be explicitly mentioned when referring to stress from now on. Lastly, void ratio within a soil element refers to the volume of voids, here fully saturated with water, over the volume of the soil grains.

The reconsolidation of liquefied sand is a problem of deformation of a water saturated porous medium. Such problems are typically modelled using a consolidation equation. The consolidation equation, introduced by Terzaghi (30), is a form of the diffusion equation, with excess pore pressure replacing density as the variable. The equation is derived using mass balance, Darcy's law, and the effective stress principle. It assumes that the soil remains at all times fully saturated, that soil grains and pore fluid are incompressible, that changes in porosity can be related in a unique way to changes in effective stress, and that the coefficients of hydraulic conductivity and one-dimensional stiffness of the soil remain constant. It is widely used in geotechnical engineering but fails to accurately predict the reconsolidation of liquefied sand (32). The equation of consolidation is discussed in depth in section 2.

Florin and Ivanov (4) introduced an alternative methodology, based on dividing the reconsolidating soil into liquified and solidified parts. Central to their framework is the observation of a boundary, known as the solidification front, between the solidified and the liquefied soil. The solidification front forms at the base of the layer and moves upwards. Its velocity was initially taken as constant, a result of using mass balance along with the assumptions of constant hydraulic conductivity and incompressibility of the solidified layer. Kolymbas (12) arrived at a similar conclusion by examining phase transitions due to compaction waves. Later research showed that the velocity of the front actually decreases as it moves closer to the surface and its position is now typically determined using empirical models, as in (11). Above the front, the soil remains liquefied and is typically considered to have zero one-dimensional stiffness (e.g. (11), (20), (25)). This assumption prevents soil grains from ever taking up any of the total load. Below the solidification front, consolidation occurs as the solidified soil is thought to have positive one-dimensional stiffness. Values for stiffness and hydraulic conductivity are often assigned to match experimental results (e.g. (11), (25), (33)). Knowing at each instant the position of the front as well as the coefficients of hydraulic conductivity and one-dimensional stiffness for the solidified soil allows the reconsolidation process to be fully recreated.

Several issues exist regarding the current state of the solidification theory. Firstly, the movement of the front is typically estimated using empirical methods, which are difficult to generalise for different types of sand. Secondly, the properties selected for the solidified soil are not realistic. Often, larger than expected values of hydraulic conductivity are required to match experimental data (e.g. (6),(28)). The use of such values is typically justified by claiming that hydraulic conductivity increases due to the loss of contacts between sand grains. However, fluidisation tests show that while such an increase is possible, it is not of significance unless effective stress reaches values below 0.1 kPa (7), a tiny fraction of the effective stress range expected for a typical reconsolidation case. An overall increase in hydraulic conductivity is not realistic.

The goal of this paper is to use the equation of consolidation throughout the reconsolidating layer, since the principle of mass balance that is in its core should apply everywhere. This goal is shown to be achievable by challenging common assumptions regarding the one-dimensional stiffness and the hydraulic conductivity of liquefied soil. The division of soil into liquefied and solidified areas appears here as a result of the modelling of soil behaviour, rather than as an externally defined condition.

2. Consolidation Equation

Consolidation equations are common in geotechnics. They are used for an array of problems, from the estimation of excess pore pressure generation on the onset of liquefaction (e.g. (5), (15)), to the evaluation of the behaviour of sediment suspensions (e.g. (21),(31)), and to the assessment of seabed response to wave loading (e.g. (20)).

In this paper, the problem of reconsolidation was studied. A fully saturated layer of liquefied sand was considered, after the end of an earthquake. A Eulerian coordinate z_0 was introduced, starting from the initial surface of the layer and pointing downwards. A soil element i was examined, whose initial depth was $z_{0\,i}$. During reconsolidation, the sand layer settled. In order to allow for finite deformation, a Lagrangian coordinate z was used, following (20). This coordinate z was defined by the initial position z_0 and the time instant t: $z(z_0, t)$. As depicted in Fig.1, it was always true at the surface of the layer that $z(0, t) = 0$. However, according to the Eulerian coordinate z_0, the surface was settling.

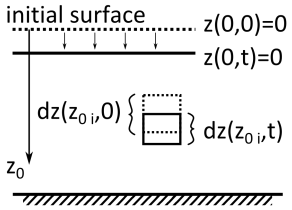

Figure 1: *z_0 is a Eulerian coordinate, starting from the initial surface of the layer and pointing downwards. z is a Lagrangian coordinate that allows for finite deformation.*

Some of the assumptions made by Terzaghi (30) are widely adopted in deriving consolidation equations. The soil is assumed to remain fully saturated at all times and the sand grains are considered incompressible. Compression and flow is often only allowed to occur in the vertical direction. Darcy's law is considered valid, at least in the case of earthquake-induced liquefaction (26). Based on these assumptions, a complete model for liquefaction is given in (15). After dropping terms that are related to the compressibility of the fluid, which is not expected to be of importance for homogeneous sand layers, a simplified equation is also proposed in (15). The terms of this simplified equation include the temporal change of pressure, the temporal change of porosity, the spacial gradient of Darcy's velocity and the temporal change of entropy. Changes in entropy due to heat generation are typically neglected for sands. Without the term for entropy, the simplified equation of (15) is equivalent to other consolidation equations used in geophysics (e.g. (5), (27)).

The consolidation equations developed in geophysics (e.g. (5), (15), (27)) cannot be readily used to predict the reconsolidation of a liquefied layer. The main issue is that they include terms for the temporal change of both pore pressure and porosity. The change in porosity cannot be easily determined and is usually assumed, in order to obtain qualitative conclusions about pore

pressures (e.g. (5), (15)). Occasionally, granular dynamics algorithms, such as the discrete element method are employed to estimate the evolution of porosity (26). However, such algorithms are not easy to implement and have limitations in the quantity of grains they can model. Even if the temporal change in porosity can be determined, the coupling between the fluid and the solid phase remains unknown. Empirical relationships are typically used to model coupling (e.g. (26)).

In geotechnical engineering, arriving at an adequately accurate solution is usually necessary. To arrive at a form of the consolidation equation that can be solved using the input parameters typically available to a geotechnical engineer, more assumptions are necessary. In particular, Terzaghi's (30) assumption that changes in porosity can be related in a unique way to changes in effective stress significantly simplifies the consolidation equation. This assumption offers a link between the temporal change of pore pressure and the temporal change of porosity. During dynamic loading, compaction is largely induced by dynamic shear, rather than by a change in effective stress. Therefore, Terzaghi's assumption is not valid and an equation that contains both the temporal change of pressure and porosity has to be used (27). However, during reconsolidation, no dynamic shear is present and the loading of sand grains is monotonic. Consequently, compaction is primarily controlled by effective stress, or equally by pore pressure. Terzaghi's assumption is now appropriate.

In this paper, in order to establish a link between effective stress and porosity, oedometer tests were used. These tests empirically relate changes in effective stress σ'_v of dry sand to changes in volume V through one-dimensional stiffness, E_0:

$$\frac{1}{V}\frac{\partial V}{\partial t} = -\frac{1}{E_0}\frac{\partial \sigma'_v}{\partial t} \tag{1}$$

Since oedometer tests were performed for dry sand, all volume change was due to change in porosity (the soil grains can be considered incompressible for the stresses examined). During reconsolidation, some volume change is necessary for the pressure of the fluid to alter. For the reconsolidating layers examined here, the bulk modulus of water was always at least two orders of magnitude larger than the one-dimensional stiffness of the soil skeleton. Therefore, the fluid was considered as incompressible and all volume change was attributed to change in porosity. Equation 1 was assumed to apply for an element within a reconsolidating layer.

Mass conservation is in the core of any consolidation equation. Any change in the mass of an element must be due to a change in the mass of water contained within it, since the grains are considered as incompressible. If A is the area of the element along a horizontal plane, V is its volume, n is porosity, (i.e. the ratio of the volume of voids V_{voids} over the volume of the element V), ρ_f is the density of the fluid, and v_{D} signifies Darcy's velocity, mass conservation can be written as follows:

$$\frac{\partial}{\partial z}\left(A\rho_f v_{\text{D}} dt\right) dz = -\frac{\partial}{\partial t}\left(\rho_f n V\right) dt \tag{2}$$

By considering the pore fluid as incompressible, ρ_f remains constant. Any change in the volume of the element (V) is equal to the change in the volume of fluid within the element (V_{voids}). Flow and compression were only allowed in the vertical direction, hence the area A of the examined element remains constant. Equation 2 is then written as:

$$\frac{\partial v_{\text{D}}}{\partial z} = -\frac{1}{V}\frac{\partial V}{\partial t} \tag{3}$$

Darcy's velocity is defined in equation 4, if u_e signifies excess pore pressure, k hydraulic conductivity, and γ_f the unit weight of the fluid that saturates the voids. It should be noted that

Darcy's velocity is relative to the soil skeleton.

$$v_D = -\frac{k}{\gamma_f}\frac{\partial u_e}{\partial z} \tag{4}$$

If σ_v is the total stress of a soil element and u_h is the hydrostatic pore pressure, then the effective stress σ'_v must be: $\sigma'_v = \sigma_v - (u_h + u_e)$. Since the total stress as well as the hydrostatic pore pressure stayed constant for an element, any change in vertical effective stress corresponded to an opposite change in excess pore pressure:

$$\frac{\partial \sigma'_v}{\partial t} = -\frac{\partial u_e}{\partial t} \tag{5}$$

Using equations 1, 4, and 5, equation 3 was written as:

$$\frac{E_0}{\gamma_f}\frac{\partial}{\partial z}\left(k\frac{\partial u_e}{\partial z}\right) = \frac{\partial u_e}{\partial t} \tag{6}$$

The void ratio e of a soil element is defined as the ratio of the volume of voids over the volume of solids within the element: $e = \frac{V_{voids}}{V_{solids}}$. Since $V = V_{voids} + V_{solids}$ and $dV = dV_{voids}$, a change in volume was expressed as a change in void ratio:

$$\frac{1}{V}\frac{\partial V}{\partial t} = \frac{1}{1+e}\frac{\partial e}{\partial t} \tag{7}$$

In equation 6, ∂z corresponds to a time instant t. As shown in Fig.1, the height $dz(z_{0\ i}, t)$ of an element i at a time instant t can be expressed as follows, regarding its initial height $dz(z_{0\ i}, 0)$:

$$\frac{dz(z_{0\ i}, t)}{dz(z_{0\ i}, 0)} = \frac{V(z_{0\ i}, t)}{V(z_{0\ i}, 0)} = \frac{e(z_{0\ i}, t) + 1}{e(z_{0\ i}, 0) + 1} \tag{8}$$

This expression allowed for partial differential equation 6 to be solved using the variable $z_0 = z(z_0, 0)$. This way, a solution always needed to be found along the initial depth of the liquefiable layer. If e_0 is the initial void ratio $e(z_{0\ i}, 0)$ of the element i in question, then the differential equation to be solved was equation 9. This equation is similar to the one derived in (20), excluding the term for contractancy. It is also equivalent to the consolidation equations typically used for the sedimentation and consolidation of a slurry, when expressed for excess pore pressure as their variable, rather than the more common void ratio (10).

$$\frac{\partial u_e}{\partial t} = \frac{E_0}{\gamma_f}\frac{\partial}{\partial z_0}\left(k\frac{\partial u_e}{\partial z_0}\frac{e_0+1}{e+1}\right)\frac{e_0+1}{e+1} \tag{9}$$

Changes in void ratio can be calculated by combining equations 1, 5, and 7:

$$\frac{\partial e}{\partial t} = \frac{1+e}{E_0}\frac{\partial u_e}{\partial t} \tag{10}$$

The only assumption of Terzaghi (30) that was not adopted was the one of constant coefficients of hydraulic conductivity and one-dimensional stiffness. This assumption of elastic soil behaviour is not realistic for a reconsolidating layer, as shown in (2).

3. Coefficient of hydraulic conductivity

The coefficient of hydraulic conductivity is considered to depend on a number of soil and fluid parameters. In (29), hydraulic conductivity k is considered a function of effective particle size D_s, unit weight of fluid γ_f, viscosity of fluid μ, void ratio e, that also depends on a particle shape factor C. The equation presented in (29) is as follows:

$$k = D_s^2 \frac{\gamma_f}{\mu} \frac{e^3}{1+e} C \tag{11}$$

In the case of reconsolidation examined here, only void ratio could change. Equation 11 was therefore written here as:

$$k = C_{Taylor} \frac{e^3}{1+e} \tag{12}$$

with C_{Taylor} introduced as a constant:

$$C_{Taylor} = D_s^2 C \frac{\gamma_f}{\mu} \tag{13}$$

Hydraulic conductivity has been shown to increase at low effective stresses. This behaviour is often used to justify large overall increases in the coefficient of hydraulic conductivity, intended to match experimental results (e.g. (6), (28), (33)). In this paper, the proposed method was assessed versus centrifuge experiments performed using Hostun sand. The data presented in (7), recorded during fluidisation tests of Hostun sand, show that the increase in hydraulic conductivity is less than 20% and only occurs for effective stresses below 0.1 kPa. In order to factor this dependence on effective stress, equation 12 was written as:

$$k = C_{Taylor} \frac{e^3}{1+e} \left(1 + 0.2 \exp\left(-100 \sigma_v'\right)\right) \tag{14}$$

Hydraulic conductivity was not allowed to reach an infinite value at zero effective stress. The assumption of infinite hydraulic conductivity at zero effective stress is common (e.g. (7), (31)). However, it is based on extrapolation of power laws developed for higher effective stresses. While fissures can emerge at low effective stresses, an infinite value of hydraulic conductivity would require the formed paths, equivalent to small pipes, to have an infinite diameter. Such an assumption is unrealistic.

Assuming that hydraulic conductivity has a reference value of k_{ref} for a void ratio value of e_{ref}, the constant C_{Taylor} was expressed as in equation 15.

$$C_{Taylor} = k_{ref} \frac{1+e_{ref}}{e_{ref}^3} \tag{15}$$

According to equation 14, hydraulic conductivity is a function of both void ratio and effective stress. As a result, it can change with depth. Equation 9 was thus rewritten as follows.

$$\frac{\partial u_e}{\partial t} = \frac{E_0}{\gamma_f} \left(\frac{e_0+1}{e+1}\right)^2 \left(\frac{\partial k}{\partial z_0}\frac{\partial u_e}{\partial z_0} + k\frac{\partial^2 u_e}{\partial z_0^2} - k\frac{\partial u_e}{\partial z_0}\frac{1}{e+1}\frac{\partial e}{\partial z_0}\right) \tag{16}$$

4. Coefficient of 1-d compression

One-dimensional stiffness E_0 was estimated through oedometer tests. In these tests, the vertical deformation resulting from the incremental loading of a soil column was measured. Horizontal deformations were restricted. Three oedometer tests were performed. The calculated values of E_0 are shown in figure 2. In the same figure, the adopted relationship for E_0 is depicted using a continuous black line. The part of the graph corresponding to low effective stresses is shown in magnification.

At zero effective stress, most compression models predict zero one-dimensional stiffness, as stiffness is typically considered proportional to some power of effective stress (for instance, see compression models listed in (22)). The hypothesis is that at zero effective stress, the contacts between grains are lost, hence the structure of the soil skeleton can no longer provide any stiffness.

However, for contacts to be entirely lost, the soil skeleton would need to expand significantly, something that is not observed in experiments. It seems that void ratio, rather than effective stress, should be the variable related to grain contacts and resulting soil properties, as is the case for the study of sediments (e.g. (21)). In DEM (Discrete Element Method) analyses, the coordination number (average number of contacts per particle) does not necessarily drop to zero at zero effective stress (e.g. (26)). A contact between two grains can exist, even if there is no contact force. One-dimensional stiffness, unlike the shear modulus, requires only the existence of contacts, not the existence of contact forces.

In this paper, E_0 was assumed to have a real, positive value at zero effective stress. A similar approached was followed in (20), where the progressive liquefaction and subsequent solidification of the seabed due to wave loading was examined. In (20), a transitional layer, where one-dimensional stiffness was not zero at zero effective stress, was introduced between the liquefied and the solidified soil. The solidification front moved based on the results of the consolidation equation within the transitional layer. Here, we did not use the device of a transitional layer. Instead, non-zero stiffness at zero effective stress was considered as the default soil behaviour. This assumption allowed the consolidation equation to be applied throughout the reconsolidating soil, without dividing it in layers. Moreover, it did not significantly affect the behaviour of the liquefied soil, where the constant hydraulic gradient restricted pore pressure change before the arrival of the solidification front. The initial value of E_0 was important for capturing the advancement of the front correctly.

One-dimensional stiffness was measured as a function of effective stress for $e \approx 0.841$ (fig. 2). Stiffness is also a function of void ratio. Void ratio dependence was adopted from (8). One-dimensional stiffness E_0 at void ratio e was related to stiffness at $e = 0.841$ ($E_{0\ (e=0.841)}$):

$$E_0 = \frac{0.841^2}{1.841}\left(\frac{1+e}{e^2}\right) E_{0\ (e=0.841)} \tag{17}$$

The expression for one-dimensional stiffness used here for Hostun sand is presented below. The effective stress range was divided in three parts. The stiffness at stresses below 0.5 kPa is defined in equation 18, with σ'_v in kPa. Stiffness at this range was crucial for the advancement of the solidification front. A similar assumption for stiffness, with non-zero stiffness at zero effective stress, is given in (14).

$$\sigma'_v \leq 0.5\ kPa: \quad E_0(kPa) = \frac{0.841^2}{1.841}\left(\frac{1+e}{e^2}\right)\left(150 + 1000\sigma'_v\right) \tag{18}$$

Above the threshold of 0.5 kPa and up to 3 kPa, a transitional phase was introduced. Stiffness there was in agreement with oedometer tests estimations (fig. 2).

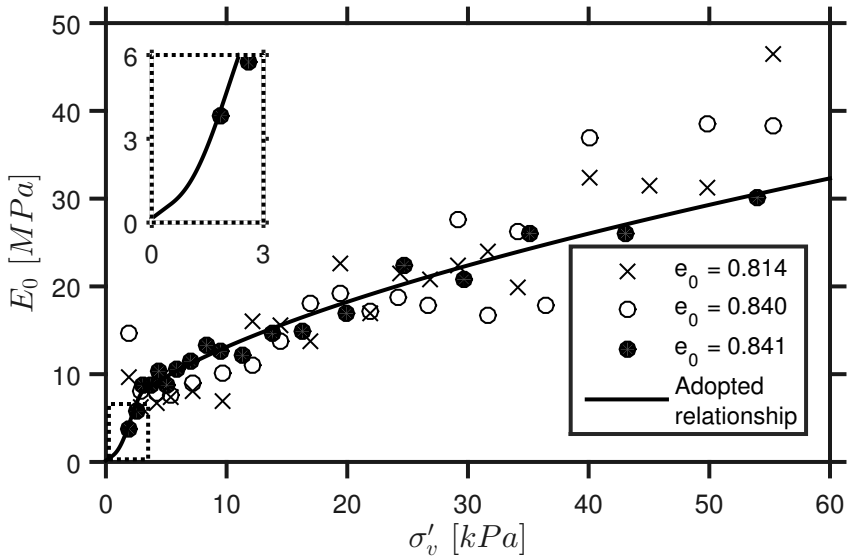

Figure 2: *One-dimensional tangent stiffness versus effective stress. Comparison of adopted expression with calculations from oedometer tests. The part of the graph corresponding to low effective stresses is shown in magnification.*

$$
\begin{aligned}
&0.5\ kPa < \sigma'_v \leq 3\ kPa: \\
&E_0(kPa) = \frac{0.841^2}{1.841}\left(\frac{1+e}{e^2}\right) \\
&\cdot\left(150 + 1000\sigma'_v + 2500(\sigma'_v)^{0.6}\cdot\frac{1}{2}\left(1-\cos\left(\pi\frac{\sigma'_v - 0.5}{3-0.5}\right)\right)\right)
\end{aligned}
\tag{19}
$$

For effective stress above 3 kPa stiffness was defined to match the oedometer data (fig. 2).

$$
\sigma'_v > 3\ kPa: \quad E_0(kPa) = \frac{0.841^2}{1.841}\left(\frac{1+e}{e^2}\right)\left(3150 + 2500(\sigma'_v)^{0.6}\right) \tag{20}
$$

Knowing the state of an element (the effective stress σ'_v and the void ratio e), the expressions for E_0 (equations 18, 19, 20) can be used to define stiffness in equation 16.

5. Numerical solution

The finite difference method was used to produce a numerical solution of equation 16. Hydraulic conductivity was considered to be a function of both void ratio e and effective stress σ'_v:

$$
\frac{\partial k}{\partial z_0} = \frac{\partial k}{\partial e}\frac{de}{dz_0} + \frac{\partial k}{\partial \sigma'_v}\frac{d\sigma'_v}{dz_0} \tag{21}
$$

The expressions of $\frac{\partial k}{\partial e}$ and $\frac{\partial k}{\partial \sigma'_v}$ were calculated from equation 14. At the beginning of the simulation, when $t = 0\ s$, the profiles of excess pore pressure $u_e(z_0, 0)$ and void ratio $e(z_0, 0) = e_0$

with depth z_0 were known. The values of dt and dz_0 were chosen before the solution ($dt = 0.2\ s$ and $dz_0 = 0.1\ m$). The following variables were defined:

$$\begin{aligned} D &= \frac{dt}{dz_0}\frac{E_0}{\gamma_f}\left(\frac{1+e_0}{1+e}\right)^2 \\ E &= \left(\frac{\partial k}{\partial e} - \frac{k}{1+e}\right)\frac{\partial e}{\partial z_0} + \frac{\partial k}{\partial \sigma'_v}\frac{d\sigma'_v}{dz_0} \end{aligned} \tag{22}$$

Using the above expressions, three more variables were defined:

$$\begin{aligned} A &= -\frac{k}{dz_0}D \\ B &= 1 + \left(\frac{2k}{dz_0} + E\right)D \\ C &= -\left(\frac{k}{dz_0} + E\right)D \end{aligned} \tag{23}$$

Equation 16 was be written as follows in a finite difference form:

$$\begin{aligned} u_e(z_0, t) =& A \cdot u_e(z_0 - dz_0, t + dt) \\ &+ B \cdot u_e(z_0, t + dt) \\ &+ C \cdot u_e(z_0 + dz_0, t + dt) \end{aligned} \tag{24}$$

Equation 24 was solved at each time step for all the soil elements within the layer. At the end of the step, the state of each element (e and σ'_v) was updated. In order to find the new value of void ratio, equation 10 was used.

At the boundaries of the layer, certain conditions applied. At the surface, excess pore pressure was always equal to zero ($u_e(0, t) = 0$) and at the base of the layer ($z_0 = D$) no flow occurred ($\frac{\partial u_e(D,t)}{\partial z_0} = 0$). Incorporating these boundary conditions at each time step, the system of equations presented in equation 25 was solved in a manner similar to (23). Variable F was defined as follows: $F = B + C$.

$$\begin{bmatrix} 1 & 0 & 0 & 0 & . & . & . & . \\ A & B & C & 0 & . & . & . & . \\ 0 & A & B & C & . & . & . & . \\ & & & . & . & . & & \\ . & . & . & . & A & B & C & 0 \\ . & . & . & . & 0 & A & B & C \\ . & . & . & . & 0 & 0 & A & F \end{bmatrix} \times \begin{bmatrix} u_e(0, t + dt) \\ u_e(dz_0, t + dt) \\ u_e(2dz_0, t + dt) \\ ... \\ u_e(D - 2dz_0, t + dt) \\ u_e(D - dz_0, t + dt) \\ u_e(D, t + dt) \end{bmatrix} = \begin{bmatrix} u_e(0, t) \\ u_e(dz_0, t) \\ u_e(2dz_0, t) \\ ... \\ u_e(D - 2dz_0, t) \\ u_e(D - dz_0, t) \\ u_e(D, t) \end{bmatrix} \tag{25}$$

6. Centrifuge tests

Geotechnical centrifuge experiments allow the stress-strain behaviour of soils to be represented accurately within a scaled-down model, through scaling up the acceleration of gravity (19).

Two centrifuge experiments (OA2 and OA3) were performed, in which the reconsolidation of liquefied sand layers was modelled. Both represented plane strain problems. Their main purpose was to examine the undrained behaviour of sand within a chamber versus that of a 'free-field' soil column. Figure 3 depicts a cross-section of these tests. The dimensions correspond to the prototype modelled, rather than the scaled-down experiment. The left array of instruments was

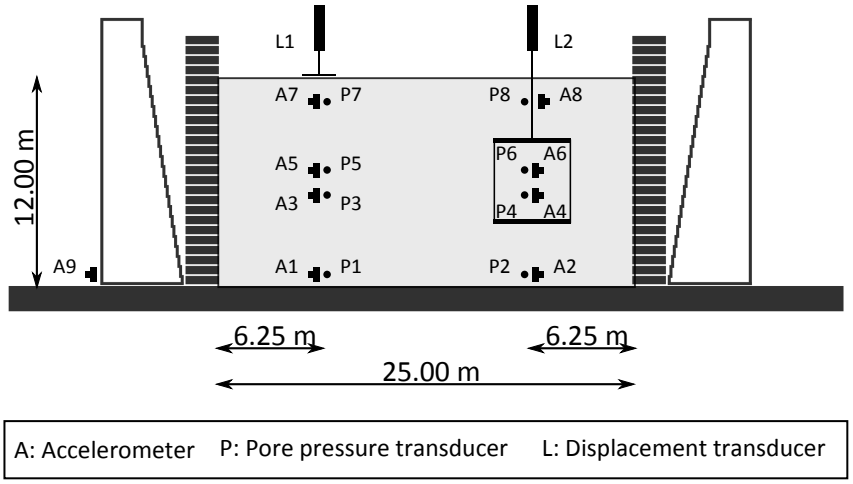

Figure 3: *Sketch of centrifuge experiments OA2 and OA3. The instrumented soil column to the left is examined. Dimensions are in prototype scale*

used to record the data presented here (pressure transducers P1, P3, P5, P7, and displacement transducer L1).

The experiments were performed on the Turner Beam Centrifuge, at the Schofield Centre of the University of Cambridge. The layers were prepared by air pluviation of Hostun sand, using the automatic sand pourer described in (17). The targeted relative density was 40%. The instrumentation consisted of miniature piezoelectric accelerometers, pore pressure transducers (PPTs), and linear variable displacement transducers (LVDTs). In order to overcome the inconsistency that exists between the scaling laws of dynamic and seepage time in centrifuge modelling (19) a high viscosity aqueous solution of hydroxypropyl methylcellulose was used for the saturation of the sand layers. The centrifugal acceleration applied was 50 g, so the targeted viscosity of the pore fluid was 50 cSt. However, since the hydroxypropyl methylcellulose solution is sensitive to temperature (1) and the centrifuge chamber is not temperature controlled, the actual measured viscosities were 42 cSt and 37 cSt for tests OA2 and OA3 respectively. The model container was a laminar box, which consists of horizontal sections that could move relative to one another, reducing boundary effects. A stored angular momentum actuator (16) was used to generate sinusoidal pseudo-harmonic input motions. Two successive earthquakes were performed per test.

An adjusted time history for L1 was considered. LVDT L1 measured the settlement of a thin, light plate resting on the surface of the soil. Apart from its own weight, this plate also supported a metal spindle that extended to the instrument. The metal plate settled into the soil, especially since the surface of the layer remained liquefied for the whole duration of the reconsolidation process. The original LVDT measurement was larger than the actual settlement of the surface. In order to quantify this adjustment, data from a third centrifuge test, OA6, was used.

In test OA6, a cross-section of which is given in figure 4, the response of a structure resting on a shallow liquefiable layer was captured. This test was performed in a rigid container, one side of which consisted of a Perspex window. Soft material was placed at the edges of the layer to limit boundary effects. A high frame-rate camera captured the seismic response through the Perspex. The produced images were used for PIV analysis (34), that allowed the estimation of displacements through the captured images. A comparison of surface settlement during reconsolidation, as

captured by LVDT L2 (figure 4) and as calculated using PIV is given in figure 5. PIV data are only available for a short duration due to the limited internal storage of the camera, which imposed an upper bound on the amount of pictures captured. The rate of settlement was not significantly different for the two methods. A picture taken after the end of the reconsolidation process allowed the estimation of the final surface settlement. The maximum reconsolidation settlement according to PIV was 75% of the total settlement captured by the LVDT during the reconsolidation process. An adjusted curve for the LVDT settlement was calculated to match PIV results (fig. 5). The same adjustment method was used for the LVDT measurements of tests OA2 and OA3 to provide an estimation of surface settlement.

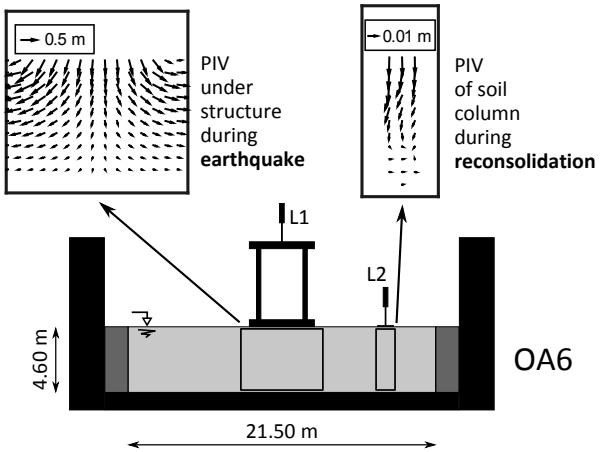

Figure 4: *Sketch of centrifuge test OA6. PIV calculated displacements for the duration of the earthquake are depicted for the area under the structure. Moreover, post-seismic, reconsolidation PIV displacements are shown for the soil column under L2. All dimensions are in prototype scale.*

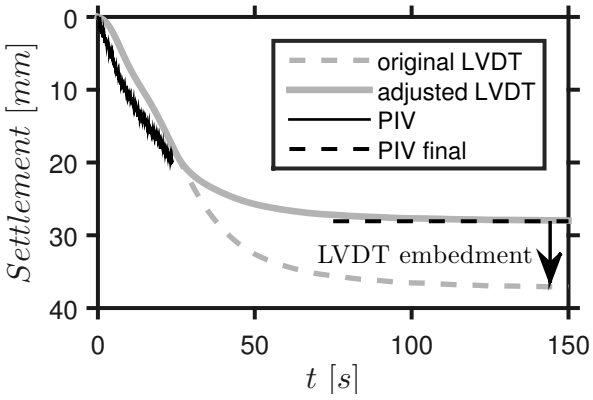

Figure 5: *Reconsolidation settlement for test OA6, in prototype scale. Comparison between PIV, original and adjusted LVDT records.*

7. Comparison with centrifuge tests

Before the proposed algorithm was used to predict the centrifuge test measurements, the initial conditions had to be defined. These included the initial distribution of void ratio and excess pore pressure with depth. The targeted void ratio of the sand layers in the centrifuge tests was $e = 0.825$. Therefore, a profile of constant void ratio with depth was assumed at the beginning of the reconsolidation process, with $e(z_0, 0) = 0.825$. This assumption is more appropriate for the beginning of the earthquake than for the beginning of the reconsolidation process. Nevertheless, it was used as it was not possible to reliably estimate the actual void ratio profile after the earthquake. The unit weight of the soil deposit was calculated based on the void ratio profile. The excess pore pressure distribution at the beginning of the reconsolidation process was estimated using the measurements recorded by PPTs. Figure 6 presents the isochrones of excess pore pressure during reconsolidation, at intervals of 20 s. The first one, corresponding to 0 s, is the initial distribution.

The constant C_{Taylor} also had to be defined, as it was necessary for the calculation of hydraulic conductivity (equation 14). By combining equations 3 and 4, the following expression was written for a soil element:

$$\frac{1}{V}\frac{\partial V}{\partial t} = \frac{\partial}{\partial z}\left(\frac{k}{\gamma_f}\frac{\partial u_e}{\partial z}\right) \tag{26}$$

Equation 26 shows that as long as the excess pore pressure dissipation process is captured reasonably well, the rate of settlement depends primarily on the coefficient of hydraulic conductivity. Hydraulic conductivity, and hence C_{Taylor}, can be hard to accurately measure directly. The settlement rate recorded by LVDT L1 was used to estimate C_{Taylor}. The values of C_{Taylor} selected were 0.001942 $\frac{m}{s}$ and 0.002418 $\frac{m}{s}$, for tests OA2 and OA3, respectively.

Having critically viewed the practice of picking values to match experimental data, the values of C_{Taylor} presented above had to be assessed. For both tests, the applied centrifugal acceleration was 50 g. The measured viscosities of the pore fluid were 42 cSt and 37 cSt for tests OA2 and OA3 respectively. These values were the average of viscosity measurements performed before and after each test. Correcting for viscosity when calculating the values of the coefficient of hydraulic conductivity k_{ref} for a reference void ratio $e_{ref} = 0.825$, the C_{Taylor} values mentioned above yielded $k_{ref} = 5.01 \cdot 10^{-4}$ $\frac{m}{s}$ for test OA2 and $k_{ref} = 5.51 \cdot 10^{-4}$ $\frac{m}{s}$ for test OA3. These values are close enough to be within the band of possible error in viscosity measurements. The assumption of a coefficient of hydraulic conductivity of $k_{ref} \approx 5 \cdot 10^{-4}$ $\frac{m}{s}$ at a value of void ratio $e_{ref} = 0.825$ for Hostun sand was a sensible one. Hazen's equation gives a value of $k \approx 8 \cdot 10^{-4}$ $\frac{m}{s}$ for Hostun sand. This rough estimation is close to the reference value used. Notably, the values of hydraulic conductivity used were not multiples of what one might expect, as is often the case in reconsolidation analyses (e.g. (6), (28)).

Good agreement with experimental results was achieved. Figure 6 depicts isochrones of excess pore pressures with depth. For both tests the prediction matched the experiment reasonably well. In the case of the deepest PPT, dissipation occurred slightly faster than predicted. This can be seen more clearly in figure 7, where the time histories of excess pore pressure dissipation captured by PPTs are plotted along with the predictions of the algorithm. Reconsolidation settlement time histories are presented in figure 8. As expected from the choice of the coefficient of hydraulic conductivity, the rate of settlement is captured reasonably well. The final value of predicted settlement matches the adjusted LVDT trace. The LVDT measurements were adjusted as detailed in section 6 to account for the settlement of the LVDT plate into the sand.

The same plots for the second, stronger earthquake of both tests are given in figures 9, 10, and 11. In all cases, the predictions captured the measurements reasonably well. The only time

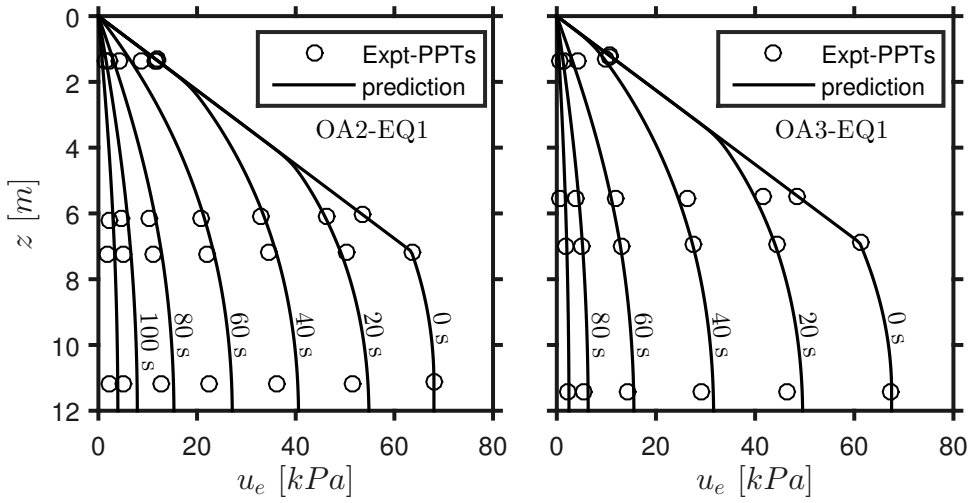

Figure 6: *Excess pore pressure dissipation isochrones for the first earthquake of both tests. The isochrones are plotted at 20 s intervals. All units in prototype scale.*

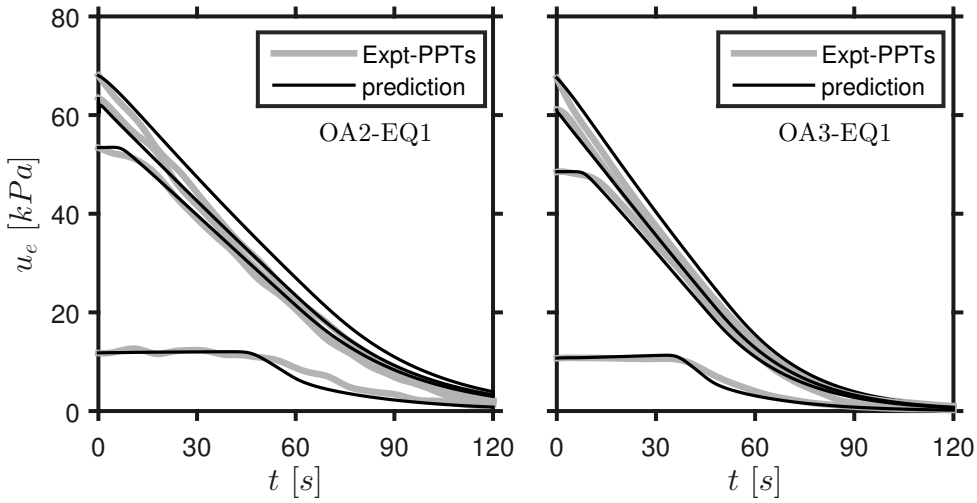

Figure 7: *Excess pore pressure dissipation time histories for the first earthquake of both tests. All units in prototype scale.*

history that was not matched as well was that of L1 for the second earthquake of test OA3 (fig. 11). LVDT L1 did not settle as much at the beginning of reconsolidation. The rate of settlement was captured adequately. Since this behaviour was not observed in any other case, it is possible that the instrument, rather than the prediction was at fault.

The centrifuge test data used in this section are available as electronic supplementary material to this paper.

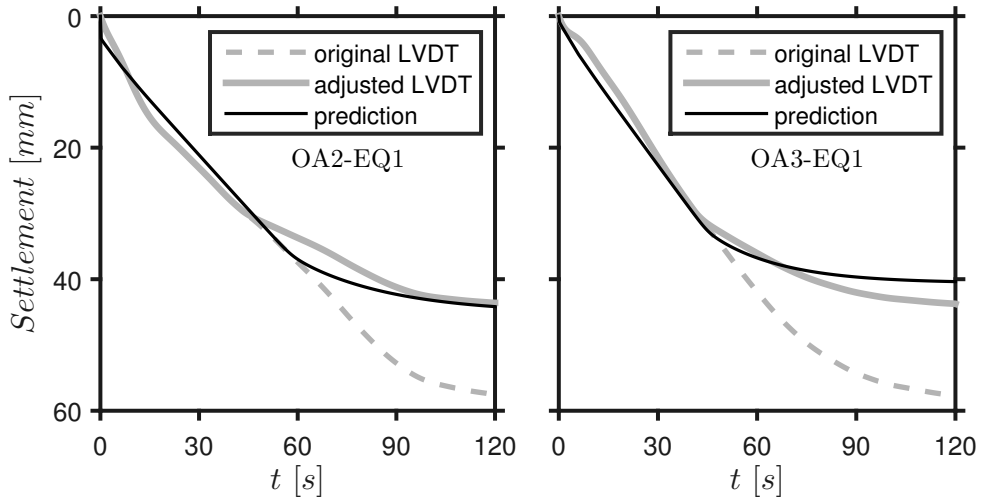

Figure 8: *Reconsolidation settlement time histories for the first earthquake of both tests. All units in prototype scale. The LVDT traces are adjusted as detailed in section 6.*

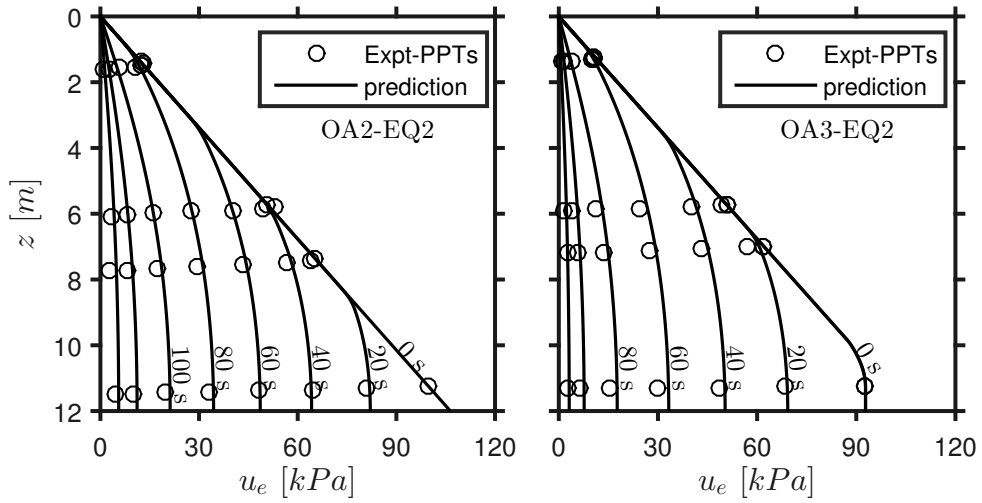

Figure 9: *Excess pore pressure dissipation isochrones for the second earthquake of both tests. The isochrones are plotted at 20 s intervals. All units in prototype scale.*

8. Discussion

The proposed algorithm was shown to predict the reconsolidation of liquefied sand layers, as recorded in geotechnical centrifuge experiments, with adequate accuracy (section 7). Linking changes in porosity to changes in effective stress through one-dimensional stiffness seems an acceptable assumption in the case of reconsolidating layers.

In order to better observe the behaviour of the proposed algorithm, a case of reconsolidation was run, using the same soil properties as those for the first earthquake of centrifuge test OA2, with the exception of assuming full liquefaction of the sand layer as the initial condition.

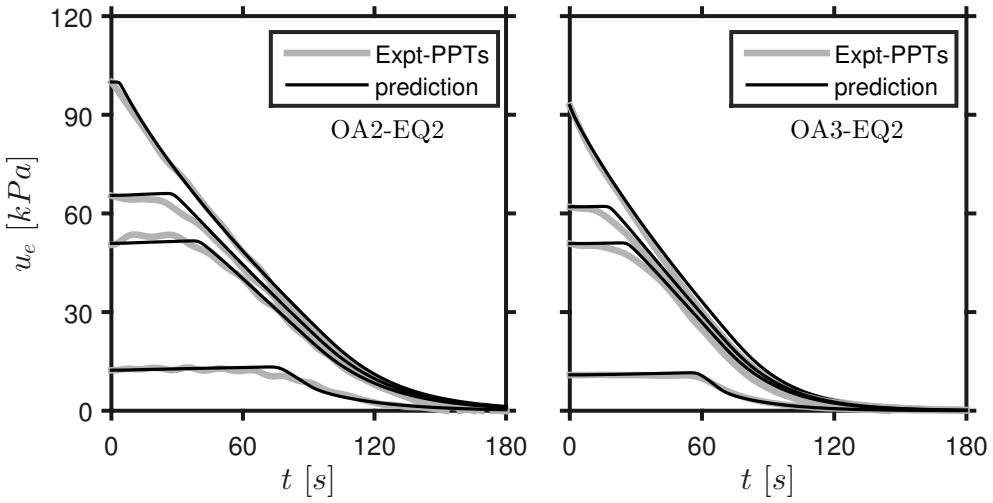

Figure 10: *Excess pore pressure dissipation time histories for the second earthquake of both tests. All units in prototype scale.*

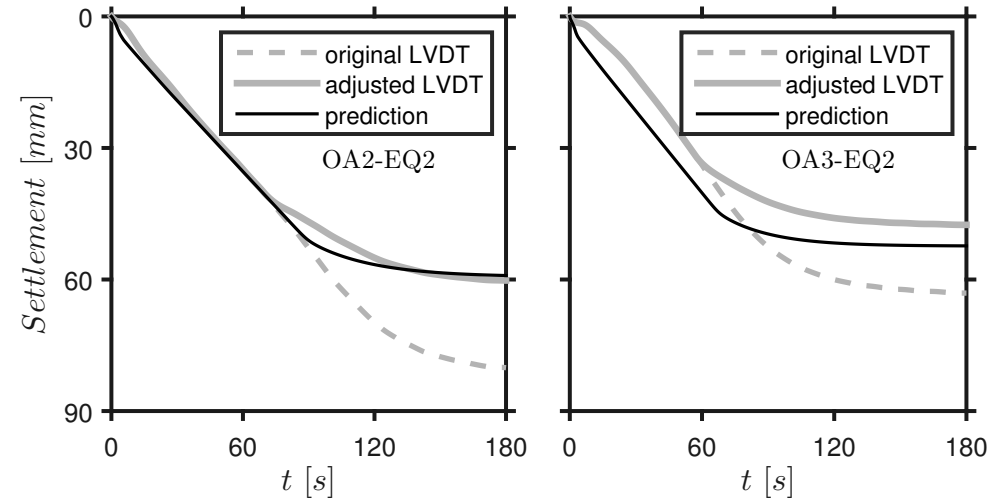

Figure 11: *Reconsolidation settlement time histories for the second earthquake of both tests. All units in prototype scale. The LVDT traces are adjusted as detailed in section 6.*

The consolidation equation was applied throughout the layer, without explicitly separating the soil in liquefied and solidified parts. Real, positive values for hydraulic conductivity and one-dimensional stiffness at zero effective stress permitted the use of the consolidation equation even for fully liquefied soil. Isochrones of excess pore pressure are shown in figure 12a and isochrones of vertical effective stress are shown in figure 12b. The position of the solidification front for each isochrone is plotted as a grey dot. The location of the front corresponds to the deepest point for which σ'_v remains practically zero. The front started from the base of the liquefied layer and advanced upwards. Its position was not defined externally, as is often the case in reconsolidation

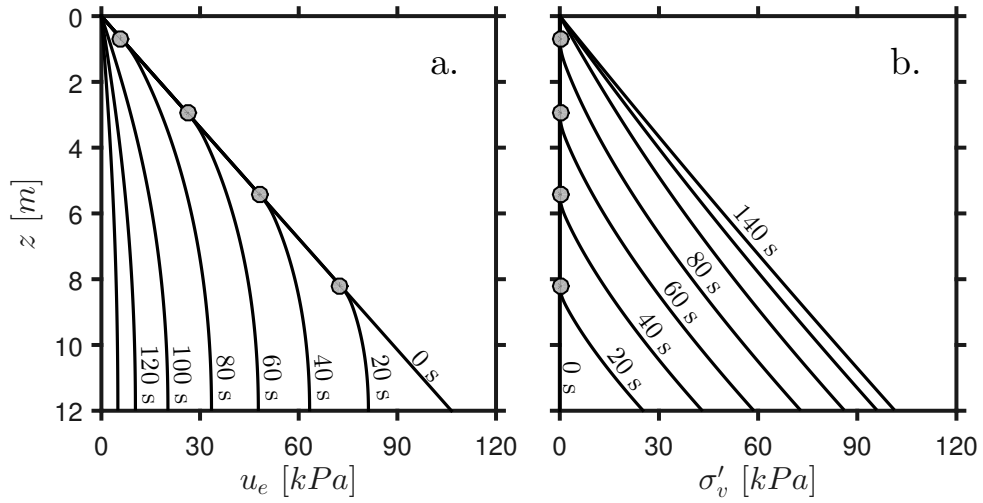

Figure 12: *Modelling of reconsolidation. Isochrones of a. excess pore pressure dissipation and b. vertical effective stress restoration. The grey dots mark the position of the solidification front.*

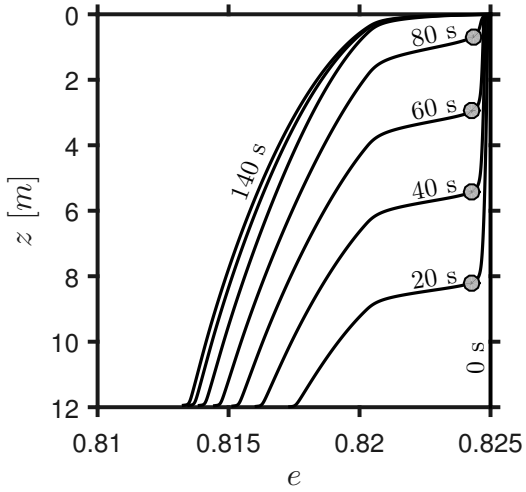

Figure 13: *Modelling of reconsolidation. Isochrones of void ratio. The grey dots mark the position of the solidification front.*

analyses (e.g. (11), (33)).

The values of hydraulic conductivity and one-dimensional stiffness at very low effective stresses were crucial for the advancement of the solidification front. Above the solidification front, the hydraulic gradient, corresponding to the slope of the isochrones of figure 12a, was constant at its maximum value, equal to the buoyant unit weight of the soil. Below the front, it was smaller. This spatial change of hydraulic gradient at the point of the solidification front led to a spatial change in Darcy's velocity (equation 4), which in turn caused volume compaction (equation 3). Hydraulic conductivity at very low effective stress was used to calculate the volume change due to the variation of the hydraulic gradient. Significant compaction was observed underneath the

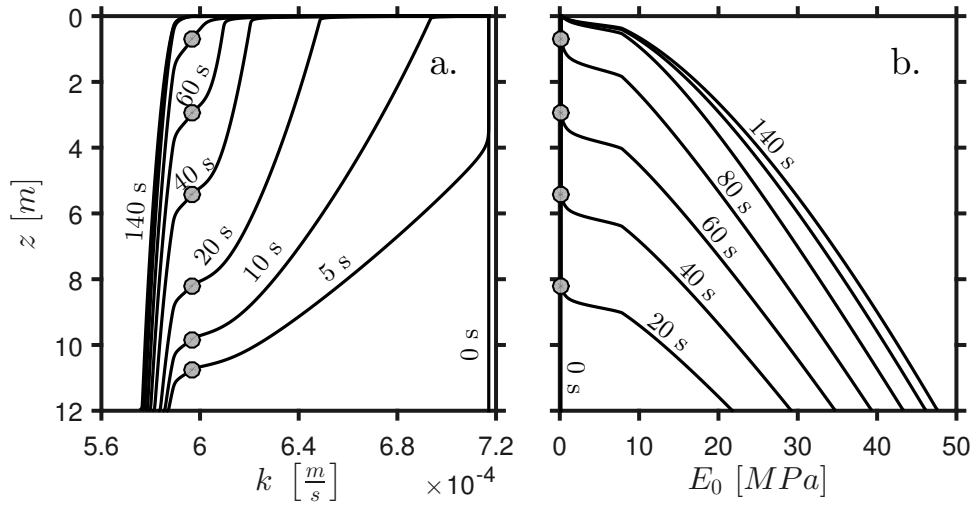

Figure 14: *Modelling of reconsolidation. Isochrones of a. hydraulic conductivity and b. one-dimensional stiffness. The grey dots mark the position of the solidification front.*

solidification front (fig. 13). Similar drops in void ratio under the solidification front have been observed before (20). Volume compaction at the area of the front was corresponded to changes in excess pore pressure, through the value of one-dimensional stiffness for very low effective stresses. The drop in pore pressure at the solidification front for one instant defines the hydraulic gradients for the next, thus controlling the advancement of the front. It is clear that the properties of liquefied soil are critical in capturing the movement of the solidification front.

Hydraulic conductivity reduced rapidly but its variation did not significantly affect the reconsolidation process. Profiles of hydraulic conductivity are given in figure 14a. The initial value quickly diminished. A drop occurred even above the solidification front. This behaviour was due to the very high sensitivity of hydraulic conductivity at very low effective stresses (7). A front related to hydraulic conductivity advanced upwards, faster that the solidification front. The solidification front exists primarily due to the change in hydraulic gradient with depth. The hydraulic conductivity front occurred due to the spatial change in hydraulic conductivity, which led to a change in Darcy's velocity, albeit much smaller than the one related to changes in hydraulic gradient (equation 4). When reconsolidation began at the base of the layer, an area of increased effective stress and hence of reduced hydraulic conductivity appeared. The interface below which hydraulic conductivity was smaller advanced even within the liquefied soil because a slight change in Darcy's velocity can be caused from hydraulic conductivity variation (equation 3). Small volume reductions above the solidification front were caused as a consequence (fig. 13). On the arrival of the solidification front, k dropped more dramatically, due to the localised densification of sand. Overall, the change in hydraulic conductivity, from $7.2 \cdot 10^{-4}$ $\frac{m}{s}$ to about $5.8 \cdot 10^{-4}$ $\frac{m}{s}$, was small. Even if hydraulic conductivity was assumed to be a constant, the results regarding excess pore pressures and deformations would not have been vastly different.

The variation of one-dimensional stiffness was primarily responsible for the accurate modelling of excess pore pressures. The isochrones for one-dimensional stiffness with depth are shown in figure 14b. Above the solidification front, one-dimensional stiffness retained its minimum value. When the solidification front arrived at a certain height, the stiffness modulus E_0 rose significantly, both due to the increase in effective stress and due to localised densification. In the areas below

the solidification front, stiffness continued to increase throughout the consolidation process, as effective stresses rose and the sand became denser. Figure 14b reveals the primary reason why the proposed algorithm, despite following most of Terzaghi's assumptions (30), yielded different results. It is unrealistic to assume that soil behaviour during reconsolidation is linear elastic. One-dimensional stiffness needs to be defined as a function of effective stress and void ratio. Oedometer tests are an easy way to get estimations of one-dimensional stiffness.

9. Conclusions

Historically, the post-seismic reconsolidation of liquefied sand layers is fragmented in two consecutive processes that are separately modelled: solidification and consolidation. Firstly, the advancement of the solidification front, which separates liquefied from solidified soil, is determined. The advancement of the front is externally imposed, based on empirical methodologies. Then, the consolidation of the already solidified soil is addressed.

The aim of this paper was to show that reconsolidation can be accurately predicted using a consolidation equation, without externally dividing the soil in different parts. Terzaghi's original consolidation equation was revisited and its assumptions were reassessed. All original assumptions were adopted, apart from the one demanding constant coefficients of one-dimensional stiffness and hydraulic conductivity. The resulting equation was applied throughout reconsolidating layers. Changes in porosity were linked to changes in pore pressure through one-dimensional stiffness, determined using oedometer tests. The proposed equation should not be used for dynamic loading, when volume compaction occurs primarily as a result of shearing.

One-dimensional stiffness and hydraulic conductivity were defined as functions of both effective stress and void ratio. Common assumptions of zero one-dimensional stiffness and infinite hydraulic conductivity at zero effective stress were not adopted. In the case of E_0, we assumed that part of the soil skeleton remained in place even at zero effective stress, providing a non-zero value for one-dimensional stiffness. This would not have been the case for the shear modulus, which does not require only the existence of grain contacts, but also of contact forces. Regarding k, we assigned a real value at zero effective stress, as 'pipes', or fissures, of infinite diameter would have been required for it to reach infinity. Those initial values of stiffness and hydraulic conductivity were crucial for capturing the advancement of the solidification front.

The solidification front was present, even though it was not explicitly defined. It manifested as a result of the modelling of soil behaviour. There was no need for complex models that determine its position. Nevertheless, complexity was added in the definition of one-dimensional stiffness at very low effective stresses. In absence of measurements, one-dimensional stiffness at zero effective stress was selected to capture the advancement of the solidification front.

The proposed algorithm, with the selected definition of parameters, captured the reconsolidation process observed in two geotechnical centrifuge tests in a satisfactory manner. The variation of one-dimensional stiffness was of most importance. Reconsolidation cannot be captured by a typical consolidation analysis because of the assumption of linear elasticity, according to which one-dimensional stiffness is a constant. While a changing coefficient of hydraulic conductivity also influences reconsolidation, its contribution is of less significance, due to the limited range of its values.

The reconsolidation of sand layers offers a good opportunity to study the behaviour of liquefied soil without having to account for dynamic loading. Here, the temporal change of porosity and pore pressure were linked through one-dimensional stiffness. This link was easily determined using a common test (the oedometer) and achieved good agreement with experimental data. However, it is still empirical. Further research is necessary into the deformations of the granular

matrix and its coupling with the fluid phase.

References

[1] Adamidis O, Madabhushi SPG. 2015. Use of viscous pore fluids in dynamic centrifuge modelling. *International Journal of Physical Modelling in Geotechnics*, **15**:3, 141–149. (doi:10.1680/ijpmg.14.00022). http://www.icevirtuallibrary.com/content/article/10.1680/ijpmg.14.00022.

[2] Brennan AJ, Madabhushi SPG. 2011. Measurement of Coefficient of Consolidation During Reconsolidation of Liquefied Sand. *Geotechnical Testing Journal*, **34**:2. (doi:10.1520/GTJ102914). http://www.astm.org/doiLink.cgi?GTJ102914.

[3] , Casagrande A, 1936. *Characteristics of Cohesionless Soils Affecting the Stability of Slopes and Earth Fills*. Harvard University.

[4] Florin VA, Ivanov PL. 1961. Liquefaction of Saturated Sandy Soils. In *Proceedings of the 5th International Conference on Soil Mechanics and Foundation Engineering, Paris, France*.

[5] Goren L, Aharonov E, Sparks D, Toussaint R. 2010. Pore pressure evolution in deforming granular material: A general formulation and the infinitely stiff approximation. *Journal of Geophysical Research*, **115**:B9. (doi:10.1029/2009JB007191). http://onlinelibrary.wiley.com/doi/10.1029/2009JB007191/abstract.

[6] Ha I, Park Y, Kim M. 2003. Dissipation Pattern of Excess Pore Pressure After Liquefaction in Saturated Sand Deposits. *Transportation Research Record* **1821**:1, 59–67. (doi:10.3141/1821-07). http://trb.metapress.com/openurl.asp?genre=article&id=doi:10.3141/1821-07.

[7] Haigh SK, Eadington J, Madabhushi SPG. 2012. Permeability and stiffness of sands at very low effective stresses. *Géotechnique* **62**:1, 69–75. (doi:10.1680/geot.10.P.035). http://www.icevirtuallibrary.com/content/article/10.1680/geot.10.p.035.

[8] Hardin, BO. 1987. 1-D Strain in Normally Consolidated Cohesionless Soils. *Journal of Geotechnical Engineering* **113**:12, 1449–1467. (10.1061/(ASCE)0733-9410(1987)113:12(1449)).

[9] Inagaki K, Iai S, Sugano T, Yamakaki H, Inatomi T. 1996. Performance of caisson type quay walls at Kobe port. *Soils and Foundations*, (Special Issue on Geotechnical Issues of the 1995 HyogokenâĂŞNambu earthquake) 119–136. http://www.pari.go.jp/bsh/jbn-kzo/jbn-bsi/taisin/paper/details/id00080.htm.

[10] Jeeravipoolvarn S, Chalaturnyk RJ, Scott JD. 2009. SedimentationâĂŞconsolidation modeling with an interaction coefficient *Computers and Geotechnics*, **36**:5, 751-âĂŞ761. (doi:10.1016/j.compgeo.2008.12.007). http://linkinghub.elsevier.com/retrieve/pii/S0266352X08001638.

[11] Kim S, Hwang J, Ko H, Kim M. 2009. Development of Dissipation Model of Excess Pore Pressure in Liquefied Sandy Ground. *Journal of Geotechnical and Geoenvironmental Eng* **135**:4. (doi:10.1061/(ASCE)1090-0241(2009)135:4(544)). http://ascelibrary.org/doi/abs/10.1061/(ASCE)1090-0241(2009)135:4(544).

[12] Kolymbas D. 1994. Compaction waves as phase transitions. *Acta Mechanica* **107**:1, 171–181. (doi:10.1007/BF01201827). http://link.springer.com/article/10.1007%2FBF01201827.

[13] Kolymbas D. 1998. Behaviour of liquefied sand. *Philosophical Transactions of the Royal Society A: Mathematical, Physical and Engineering Sciences*, **356**:1747. (doi:10.1098/rsta.1998.0289). http://rsta.royalsocietypublishing.org/cgi/doi/10.1098/rsta.1998.0289.

[14] Kolymbas D. 2015. Introduction to barodesy. *Géotechnique* **65**:1, 52–65. (doi:10.1680/geot.14.P.151). http://www.icevirtuallibrary.com/doi/abs/10.1680/geot.14.P.151.

[15] Lakeland DL, Rechenmache A, Ghanem R. 2014. Towards a complete model of soil liquefaction: the importance of fluid flow and grain motion. *Proc. R. Soc. A* **470**. (doi:10.1098/rspa.2013.0453). http://rspa.royalsocietypublishing.org/cgi/doi/10.1098/rspa.2013.0453.

[16] Madabhushi SPG, Schofield AN, Lesley S. 1998. A new Stored Angular Momentum (SAM) based earthquake actuator. *Proc. of The Intern. Conf. Centrifuge '98*, 111–116.

[17] Madabhushi SPG, Houghton NE, Haigh SK. 2006. A new automatic sand pourer for model preparation at University of Cambridge. *Physical Modelling in Geotechnics, 6th ICPMG'06*, 217–222. (doi:10.1201/NOE0415415866.ch25). http://www.crcnetbase.com/doi/abs/10.1201/NOE0415415866.ch25.

[18] Madabhushi SPG, Haigh, SK. 2012. How Well Do We Understand Earthquake Induced Liquefaction? *Indian Geotechnical Journal*, **42**:3, 150–160. (doi:10.1007/s40098-012-0018-2). http://link.springer.com/article/10.1007%2Fs40098-012-0018-2.

[19] Madabhushi SPG. 2014. *Centrifuge Modelling for Civil Engineers*. Taylor & Francis, London.

[20] Miyamoto J, Sassa S, Sekiguchi H. 2004. Progressive solidification of a liquefied sand layer during continued wave loading. *Géotechnique* **54**:10, 617–629. (doi:10.1680/geot.2004.54.10.617). http://www.icevirtuallibrary.com/content/article/10.1680/geot.2004.54.10.617.

[21] Pane V, Schiffman RL. 1985. A note on sedimentation and consolidation. *Géotechnique*, **35**:1, 69-âĂŞ72. (doi:10.1680/geot.1985.35.1.69). http://www.icevirtuallibrary.com/content/article/10.1680/geot.1985.35.1.69.

[22] Pestana JM, Whittle AJ. 1995. Compression model for cohesionless soils. *Géotechnique* **45**:4, 611–631. (doi:10.1680/geot.1995.45.4.611). http://www.icevirtuallibrary.com/content/article/10.1680/geot.1995.45.4.611.

[23] Sassa S, Sekiguchi H, Miyamoto J. 2001. Analysis of progressive liquefaction as a moving-boundary problem. *Géotechnique*, **51**:10, 847-âĂŞ857. (doi:10.1680/geot.2001.51.10.847). http://www.icevirtuallibrary.com/doi/full/10.1680/geot.2001.51.10.847.

[24] Sawicki A, MierczynÌĄski J. 2006. Developments in Modeling Liquefaction of Granular Soils, Caused by Cyclic Loads. *Applied Mechanics Reviews*, **59**:2, 91–106. (doi:10.1007/s10035-003-0151-9). http://appliedmechanicsreviews.asmedigitalcollection.asme.org/article.aspx?articleid=1398487.

[25] Scott RF. 1986. Solidification and consolidation of a liquefied sand column. *Soils and Foundations* **26**:4.

[26] Shamy U El, Zeghal M. 2007. A micro-mechanical investigation of the dynamic response and liquefaction of saturated granular soils. *Soil Dynamics and Earthquake Engineering* **27**:8, 712–729. (doi:10.1016/j.soildyn.2006.12.010). http://linkinghub.elsevier.com/retrieve/pii/S0267726107000048.

[27] Snieder R, Beukel A. 2004. The liquefaction cycle and the role of drainage in liquefaction. *Granular Matter*, **6**:1, 1-âĂŞ9. (doi:10.1007/s10035-003-0151-9). http://link.springer.com/10.1007/s10035-003-0151-9.

[28] Su D, Li X, Xing F. 2009. Estimation of the Apparent Permeability in the Dynamic Centrifuge Tests. *Geotechnical Testing Journal*, **32**:1. (doi:10.1520/GTJ100972). http://www.astm.org/doiLink.cgi?GTJ100972.

[29] Taylor DW. 1948. *Fundamentals of soil mechanics*. John Wiley and Sons, New York.

[30] Terzaghi K. 1943. *Theoretical Soil Mechanics* John Wiley and Sons, New York.

[31] Toorman EA. 1999. Sedimentation and self-weight consolidation: constitutive equations and numerical modelling. *Géotechnique*, **49**:6, 709-âĂŞ726. (doi:10.1680/geot.1999.49.6.709). http://www.icevirtuallibrary.com/content/article/10.1680/geot.1999.49.6.709.

[32] Towhata I. 2008. *Geotechnical Earthquake Engineering* Springer, Berlin, Heidelberg.

[33] Wang B, Zen K, Chen GQ, Zhang YB, Kasama K. 2013. Excess pore pressure dissipation and solidification after liquefaction of saturated sand deposits. *Soil Dynamics and Earthquake Engineering* **49**. (doi:10.1016/j.soildyn.2013.02.018). http://linkinghub.elsevier.com/retrieve/pii/S0267726113000717.

[34] White DJ, Take WA, Bolton MD. 2003. Soil deformation measurement using particle image velocimetry (PIV) and photogrammetry. *Géotechnique* **53**:7, 619–631. (doi:10.1680/geot.2003.53.7.619).